JOURNAL OF CATALYSIS 135, 173–185 (1992)

The Structure and Activity of Titania Supported Cobalt Catalysts

SUI-WEN HO,* JOSE M. CRUZ,† MARWAN HOUALLA,* AND DAVID M. HERCULES*

*Department of Chemistry, University of Pittsburgh, Pittsburgh, Pennsylvania 15260, and †Intervep, S.A., Apdo. 76343 Caracas 1070 A Venezuela

Received August 22, 1989; revised November 6, 1991

A series of titania supported cobalt catalysts (0.5–6%) were prepared by incipient wetness impregnation, and were characterized by ESCA, XRD, and hydrogen chemisorption. After calcination at 400°C, a surface $CoTiO_3$-like phase was the main species present in the 0.5 and 1% cobalt catalysts. For higher cobalt loadings, discrete Co_3O_4 particles were formed in addition to surface $CoTiO_3$. ESCA indicates that after reduction the cobalt metal particle size (6–13 nm) increases with increasing cobalt loading, but does not vary with reduction temperature (400–500°C). Hydrogen chemisorption was found to be activated and suppressed. The extent of hydrogen chemisorption suppression increases with increasing reduction temperature and decreasing cobalt particle size. The turnover frequency (based on cobalt dispersion derived from ESCA) for benzene and CO hydrogenation decreases with increasing reduction temperature and decreasing cobalt particle size. The decline in activity correlates with the extent of suppression of H_2 chemisorption. The results were interpreted in terms of a decrease in the fraction of exposed surface cobalt due to site blocking by reduced TiO_x moieties.

INTRODUCTION

It is well known that the support plays a fundamental role in determining the structure and activity of supported metal catalysts. In the past decade considerable attention has been given to the use of TiO_2 as a support, due mainly to the fact that TiO_2 exhibits the so-called Strong Metal–Support Interaction (SMSI) effect (*1*). This phenomenon is characterized by suppression of the capacity of the metal to chemisorb hydrogen after high-temperature reduction. To date, most SMSI related work has focused on titania supported Pt, Rh, and Ni (*2–4*) catalysts. Only a limited number of studies have dealt with cobalt-based systems (*3*, 5–8). Reuel and Bartholomew (*8*) have examined the effects of support and dispersion on the CO hydrogenation activity and selectivity of cobalt. However, only three Co/TiO_2 catalysts were examined. Also, the catalysts were partially reduced, a factor which may preclude an unequivocal interpretation of the effect of the support (*9*).

In the present work, ESCA, XRD, and H_2 chemisorption were employed to characterize the state and dispersion of cobalt in a series of Co/TiO_2 catalysts. The catalyst surface structure derived from this study is correlated with benzene and CO hydrogenation activities.

EXPERIMENTAL

Catalyst Preparation

The TiO_2 support (Degussa P-25, BET surface area 50 m^2/g, pore volume 0.4 cm^3/g) was wetted with distilled water, dried at 100°C for 16 h, and calcined at 400°C for 16 h before use. The catalysts were prepared by incipient wetness impregnation of the TiO_2 support with cobalt (II) nitrate (Fisher) solutions. The nominal cobalt content was varied from 0.5 to 6 wt% of the TiO_2 support. The impregnated powders were dried at 100°C for 16 h and calcined for 16 h at 400°C. The catalysts are designated as Co_xTi, where x stands for the cobalt loading. The BET surface area remained essentially constant at 47 ± 2 m^2/g

0021-9517/92 $3.00

catalyst for the calcined Co/TiO_2 catalysts. "Calcined" catalysts will also be referred to as "Oxidic" catalysts.

Reduction of Catalysts

Catalysts were reduced under hydrogen flow (50 cm^3/min, 99.999%) using two sets of conditions: 400°C for 12 h and 500°C for 1h. The lengthy treatment at 400°C was adopted to ensure complete reduction of the cobalt phase.

X-ray Diffraction (XRD)

X-ray powder diffraction patterns were obtained using a Diano XRD-6 diffractometer employing Ni-filtered Cu$K\alpha$ radiation (1.5405 Å). The X-ray tube was operated at 50 kV and 25 mA, and was scanned at 0.4 degree/min. The powdered catalysts were packed into a $2 \times 2 \times 0.2$ cm^3 hollowed-out plastic slide. The ASTM powder diffraction file was used to identify the phases present. Crystallite sizes were calculated from line broadening using the Scherrer equation (*10*).

X-ray Photoelectron Spectroscopy (XPS or ESCA)

ESCA spectra of oxidic catalysts were obtained using a Leybold–Heraeus LHS-10 electron spectrometer equipped with an Al anode (1486.6 eV) operated at 12 kV and 22 mA. ESCA measurements of reduced catalysts were performed with an AEI ES200A spectrometer. Reduction was carried out in a sealable probe to allow transfer of reduced catalysts from a tube reactor to the spectrometer without exposure to air. Appropriate calibrations were made to allow the direct comparison of XPS intensities obtained from the two instruments. The oxidic catalysts were run as powders dusted on sticky tape; catalysts mounted on a sealable probe were pressed into 6×15 mm^2 rectangular pellets at a pressure of 1000 Kg/cm^2. The $Ti2p_{3/2}$ line (B.E. 458.7 eV) from the support was used as the binding energy reference for the catalysts. The binding energies of standard compounds that do not contain Ti^{+4} were referenced to the C1*s* line (B.E. 284.6 eV).

Several models have been proposed to relate the ESCA intensity ratio (I_m/I_s) for a supported phase (m) dispersed on a carried (s) to the particle size of the supported phase (*11–13*). The validity of these models rests, however, on the assumption, not always justified, of a uniform repartition of the supported phase (i.e., similar distribution of the supported phase between the inner pores and the outer parts of the catalyst particle). In the present investigation, the model proposed by Kerkhof of Moulijn (*13*) was used to calculate the dispersion of the cobalt phase. The photoelectron cross sections and the mean escape depths used in these calculations were taken from Refs. (*14*) and (*15*), respectively. According to Kerkhof and Moulijn (*13*), for a supported phase (m) present as discrete cubic particles of a dimension (d), the ESCA intensity ratio I_m/I_s is given by the equation

$$(I_m/I_s) = (I_m^0/I_s^0)\,[1 - \exp(-d/\lambda_m)]/d/\lambda_m,$$

where λ_m is the mean escape depth of the photoelectrons in (m) and I_m^0/I_s^0 is the predicted intensity ratio for monolayer dispersion.

Hydrogen Chemisorption

Hydrogen chemisorption was performed in a conventional stainless steel volumetric system evacuated by mechanical and oil diffusion pumps. The base pressure of the system was ca. 5×10^{-6} Torr. An MKS-390 Baratron Pressure Transducer was used for pressure measurements over a range of 0 to 1000 Torr. Following reduction, the sample (ca. 1 g) was evacuated for 1 h. Following evacuation, adsorption isotherms were taken at room temperature. The total hydrogen uptake was determined by extrapolating the straight-line portion of the adsorption isotherm to zero pressure. Since H_2 chemisorption on supported cobalt catalysts was reported to be an activated process (*16*), a second isotherm was taken by raising the temperature to 185°C and then

cooling to room temperature after each equilibrium point. The extent of reduction of the cobalt phase was determined by O_2 uptake at 400°C (*17*). It is assumed that O_2 consumption is due to oxidation of Co metal to Co_3O_4.

Activity Measurements

Benzene and CO hydrogenation activity measurements were performed in a flow microreactor. The microreactor system consists of four U-shaped Pyrex glass reactors ($\frac{1}{4}$" in diameter) mounted in a four-tube furnace and connected to stainless steel feed lines equipped with pressure and flow controllers (Matheson) and an on-line gas chromatograph (Perkin-Elmer Sigma 2000). The reactor was packed with 50 mg of catalyst (ca. 6 mm in length) on top of a glass wool plug. CO hydrogenation activity was measured at 185°C. A premixed $CO/H_2/He$ (3/9/88, 99.999%) feed gas was introduced into the reactor at a flow rate of 50 cm^3/min. The products were analyzed by gas chromatography using an OV 101 column; the conversion of CO to hydrocarbons was kept below 1%. Benzene hydrogenation activity measurements were carried out at 70°C. The reactant mixture (H_2 : benzene = 98 : 2) was obtained by flowing H_2 through a benzene saturator maintained at room temperature. The reactant gas was introduced at a flow of 50 cm^3/min. Products were analyzed by gas chromatography using a column packed with 10% carbowax 400 on Chromosorb W-HP. Under these reaction conditions, conversion is below 5% and cyclohexane was the only product formed.

RESULTS

Oxidic Catalysts

X-ray diffraction (XRD). X-ray diffraction patterns characteristic of the support were observed for all catalysts. The composition of the support determined as described in Ref. (*18*) was invariant in all catalysts (70% anatase, 30% rutile) indicating that impregnation and calcination have no effect on the anatase to rutile ratio. Diffraction lines characteristic of Co_3O_4 were observed for catalysts having cobalt contents higher than 1%. The Co_3O_4 crystallite size was estimated from line broadening of the ⟨111⟩ line using the Scherrer equation (*10*). The results reported in Table 1 indicate an increase in Co_3O_4 crystallite size from 15 to 19 nm as cobalt loading increases from 1.5 to 6%.

TABLE 1

Percentage and Particle Size of Co_3O_4 Obtained from XRD

Sample	% Co_3O_4	Size of Co_3O_4 (nm)
Co1Ti	[a]	[a]
Co1.5Ti	47	15
Co3Ti	80	17
Co4Ti	83	18
Co6Ti	78	19

[a] Peak intensities are too weak to measure accurately.

The fraction of the Co phase present as crystalline Co_3O_4 was estimated by comparing the intensity ratios of lines characteristic of Co_3O_4 ⟨440⟩ and TiO_2 (rutile) ⟨310⟩ with the values obtained from physical mixtures of Co_3O_4 and TiO_2. The results, reported in Table 1, indicate that the percent of cobalt present as crystalline Co_3O_4 increases from 47 to 80% as the cobalt content of the catalysts increases from 1.5 to 3.0% and levels off at ca. 80% for higher cobalt loadings.

ESCA. The ESCA Co2*p* spectra of Co_3O_4 and $CoTiO_3$ model compounds are shown in Fig. 1. Note that the Co2$p_{3/2}$ spectrum of $CoTiO_3$ exhibits a strong shake-up satellite located 6 eV higher than the Co2$p_{3/2}$ main peak (*19*). In addition to the intense shake-up satellite, the ESCA Co2$p_{3/2}$ binding energy of $CoTiO_3$ (781.2 eV) is 1.4 eV higher than that of Co_3O_4.

Representative ESCA Co2*p* spectra of the calcined Co/TiO_2 catalysts are also shown in Fig. 1. The ESCA Co2$p_{3/2}$ binding

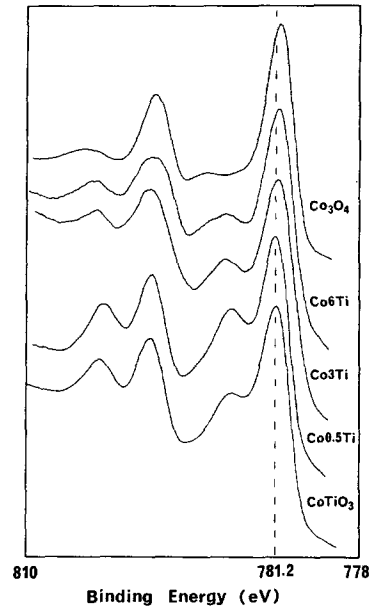

Fig. 1. ESCA $Co2p_{3/2}$ spectra of standard compounds and oxidic catalysts.

energies and the height ratios of the shake-up satellite to the main $Co2p_{3/2}$ peak (S/M) are reported in Table 2 for all catalysts. The $Co2p_{3/2}$ B.E. values and the *S/M* height ratios for Co0.5Ti and Co1Ti catalysts are consistent with the presence of $CoTiO_3$. The $Co2p_{3/2}$ B.E. values and the *S/M* height ratios of the shake-up satellite decrease with further increase in cobalt loading. In addition, the $Co2p_{3/2}$ peak becomes broader at higher cobalt loading. For Co6Ti, the $Co2p_{3/2}$ B.E. value of 780.0 ± 0.2 eV and the satellite structure are close to those of Co_3O_4.

Variation of the ESCA $Co2p_{3/2}$/Ti2*p* intensity ratio as a function of Co/Ti atomic ratio is shown in Fig. 2 (solid circles) along with the monolayer line predicted by the Kerkhof and Moulijn model (*13*). For cobalt loadings below 1.0%, the observed intensity ratios correspond to the monolayer coverage for the oxidic catalysts. Deviation from the monolayer line is observed for higher cobalt loadings indicating formation of a discrete cobalt phase.

Reduced Catalysts

ESCA. Examination of the ESCA Ti2*p* envelope for oxidic and reduced catalysts shows that no significant change occurs on reduction. This is in agreement with other studies (*20–22*).

After reduction, a peak located at 777.4 ± 0.2 eV characteristic of cobalt metal (*23*, *24*) appeared for all catalysts (Fig. 3). The degree of reduction of the cobalt phase was estimated from the ESCA $Co2p_{3/2}$ envelope according to the method of Stranick *et al.* (*23*). The results indicate complete reduction of the cobalt phase to cobalt metal at 400 and 500°C for all loadings.

Figure 2 shows the $Co2p_{3/2}$/Ti2*p* intensity ratios for catalysts reduced at 400°C. A significant decrease in the Co/Ti intensity ratio is observed on reduction. A similar decrease was obtained when catalysts were reduced at 500°C, indicating that sintering of the cobalt phase occurs on reduction. The cobalt metal particle size was calculated using the Kerkhof and Moulijn model (*13*). The results, reported in Table 2, indi-

TABLE 2

ESCA $Co2p_{3/2}$ Binding Energy, *S/M* Height Ratio for Oxidic Co/TiO_2 Catalysts and Particle Size of the Cobalt Metal in the Reduced Catalysts

Sample	$Co2p_{3/2}$		Cobalt metal particle size (nm)[d]	
	B.E.[a]	*S/M*[b]	400°C[c]	500°C[c]
Co0.5Ti	781.2	0.47	5.7 ± 1.3	5.4 ± 2.0
Co1Ti	781.1	0.45	5.6 ± 1.7	5.6 ± 2.0
Co1.5Ti	780.9	0.44	7.8 ± 0.4	8.4 ± 0.4
Co3Ti	780.4	0.33	9.5 ± 1.1	9.9 ± 0.8
Co4Ti	780.1	0.23	11.8 ± 0.5	11.0 ± 0.6
Co6Ti	780.0	0.22	12.5 ± 0.3	12.7 ± 0.8
Co_3O_4	779.8	0.13		
$CoTiO_3$	781.2	0.43		

[a] Standard deviation for B.E. measurements is ±0.2 eV.

[b] Shake-up satellite to main peak height ratios.

[c] Reduction temperature of catalysts.

[d] Co metal particle determined from Kerkhof and Moulijn model (*13*).

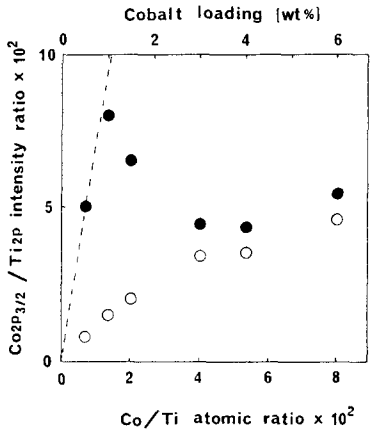

Fig. 2. Variation of ESCA Co2$p_{3/2}$/Ti2p intensity ratio as a function of cobalt loading. (●), oxidic catalysts; (○), catalysts reduced at 400°C. The dashed line gives the predicted Co2$p_{3/2}$/Ti2p intensity ratios for monolayer coverage.

cate that the cobalt metal particle size increases from 6 to 13 nm with increasing cobalt loading. The cobalt particle sizes measured by ESCA at 500°C were the same as those measured at 400°C, within experimental error. It should be noted, however, that the calculated particle size of the cobalt phase and the magnitude of the estimated increase in cobalt particle size with increasing cobalt loading are a function of the assumptions made with respect to the shape of the cobalt particles (cubic, hemispherical or spherical) (*11*).

Oxygen titration. Oxygen uptake of 6.5 and 11.5 μmol O_2/g-TiO_2 was obtained when the TiO_2 support was subjected to hydrogen treatment at 400 and 500°C respectively, along with a color change of the titania from white to light blue. This is consistent with previous studies (*20–22, 25*), and is attributed to formation of Ti^{+3} ions on reduction. The percentage of Ti^{+4} ion reduced to Ti^{+3} ion can be calculated from the oxygen uptake, based on the stoichiometry that one oxygen removed produced two Ti^{+3} ions. The results reported in Table 3 show that the percent Ti^{+3} ion increases from 0.2 to 0.4%, when the reduction temperature increases from 400 to 500°C.

The extent of cobalt reduction in the catalysts obtained from oxygen titration is reported in Table 4. Note that the extent of reduction exceeds 100%. Since ESCA data

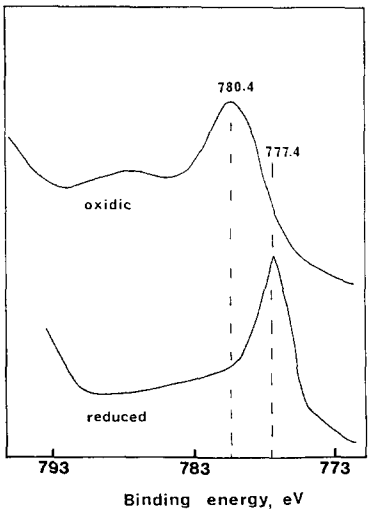

Fig. 3. ESCA Co2$p_{3/2}$ spectra for oxidic and reduced Co3Ti catalysts.

TABLE 3

Extent of Reduction of Titania Obtained from Oxygen Titration

Sample	Oxygen uptake (μmol O_2/g-TiO_2)[a]		Percentage of Ti^{+3}[b,c]	
	400°C[d]	500°C[d]	400°C[d]	500°C[d]
TiO_2	6.5	11.5	0.2	0.4
Co1.5Ti	12.8	22.2	0.4	0.7
Co3Ti	17.9	36.3	0.6	1.2
Co6Ti	31.4	56.3	1.0	1.8

[a] For catalysts, this is the amount of oxygen uptake calculated from the difference between total oxygen uptake and the amount predicted for complete reduction of cobalt.

[b] Assuming one oxygen removed by H_2 treatment generates two Ti^{+3}, calculated by: {[oxygen uptake (μmol O_2/g-TiO_2)]/[μmol Ti/g-TiO_2)} × 4.

[c] Relative standard deviation for measurement of % Ti^{+3} is ±30%.

[d] Reduction temperature.

TABLE 4

Extent of Reduction of Cobalt in Co/TiO_2 Catalysts Obtained from Oxygen Titration

Sample	Percent reduction of cobalt[a]	
	400°C[b]	500°C[b]
Co1.5Ti	103	113
Co3Ti	105	110
Co6Ti	105	109

[a] Standard deviation for measurement from oxygen titration is ±2%.

[b] Reduction temperature of catalysts.

indicate complete reduction of cobalt, the "excess" reduction (i.e., the "excess" oxygen uptake (Table 4)) can be attributed to partial reduction of titania. The percent Ti^{+3} ion formed in the catalysts can be calculated from the "excess" oxygen uptake. The results reported in Table 3 show up to fourfold increase in the percentage of Ti^{+4} ion reduced to Ti^{+3} ion compared to that of the titania carrier without cobalt.

Hydrogen chemisorption. The results of H_2 chemisorption are shown in Table 5. The observed hydrogen uptake measured at room temperature (1.2–6.3 μmol/g-Cat.) corresponds to cobalt particle sizes in the range of 75–190 nm. Clearly, the cobalt particle sizes are too large considering the cobalt loading and the titania surface area (50 m^2/g). By raising the cell temperature to 185°C and cooling to room temperature during adsorption, the total hydrogen uptake is enhanced up to twofold. This indicates that hydrogen chemisorption is activated for titania supported cobalt catalysts (*16*). Thus, the cobalt dispersion given in Table 5 was calculated from total H_2 uptake measured after raising the cell temperature to 185°C (assuming that the adsorption stoichiometry H/Co_s is equal to 1).

The variation of cobalt dispersion as a function of cobalt loading for various reduction temperatures is shown in Fig. 4, along with cobalt dispersions calculated from ESCA data. It is clear that cobalt dispersion calculated from hydrogen chemisorption data increases with increasing cobalt loading. This is contrary to what one would expect on the basis of the method used for catalyst preparation. It is also at variance with the ESCA data which show a decrease in cobalt dispersion with increasing cobalt loading. Note also that H_2 chemisorption data indicate a decrease in cobalt dispersion with increasing reduction temperature, whereas ESCA results (Table 2) show that the cobalt particle size is not significantly changed as a function of reduction temperature. Therefore, it is concluded that H_2 chemisorption is suppressed, and is inappropriate for estimating the cobalt particle size. This is consistent with early studies of titania supported cobalt catalysts (*5–7*).

Catalytic activity. The variation of benzene and CO hydrogenation activity as a function of time on stream for 3% Co/TiO_2 at various reduction temperature, is shown in Fig. 5. Generally, an initial decrease in activity was observed, then a steady state

TABLE 5

Hydrogen Uptake at Various Reduction Temperatures

Sample	Reduction temp. 400°C Uptake (μmol H_2/g-cat.)		Reduction temp. 500°C Uptake (μmol H_2/g-cat.)	
	R.T.[a]	activated[b]	R.T.[a]	activated[b]
Co1.5Ti	[d]	1.9 ± 0.3 (1.6 ± 0.2)[c]	[d]	1.0 ± 0.2 (0.8 ± 0.2)[c]
Co3Ti	3.4 ± 0.1	4.9 ± 1.3 (2.0 ± 0.6)[c]	1.2 ± 0.1	2.1 ± 0.9 (0.9 ± 0.4)[c]
Co4Ti	5.2 ± 0.5	8.0 ± 1.2 (2.4 ± 0.4)[c]	1.8 ± 0.2	3.5 ± 0.7 (1.1 ± 0.2)[c]
Co6Ti	6.3 ± 0.6	14.2 ± 2.1 (3.0 ± 0.4)[c]	3.8 ± 0.4	7.3 ± 0.8 (1.6 ± 0.2)[c]

[a] Uptake measured at room temperature.

[b] Uptake also measured at room temperature after the cell temperature was raised to 185°C and cooled to room temperature at each hydrogen pressure.

[c] Number in parenthesis represents percent dispersion of cobalt metal calculated from H_2 adsorption (stoichiometry $H/Co_s = 1$).

[d] Uptake is too small to make accurate measurements.

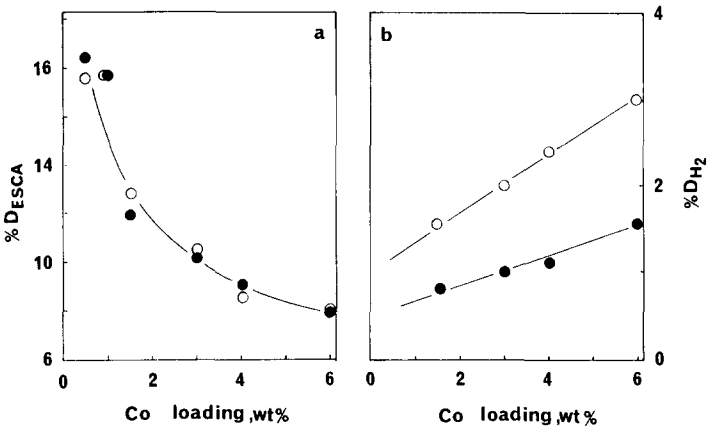

Fig. 4. Variation of cobalt dispersion calculated from ESCA data (a) and H_2 chemisorption (b) as a function of cobalt loading. (○), catalysts reduced at 400°C; (●), catalysts reduced at 500°C.

was gradually reached after 6 h on stream. The initial and steady state activities for benzene and CO hydrogenation are given in Tables 6 and 7, respectively. In general, the steady state activity (8 h on stream) is ca. 40–60% of the initial activity.

The variation of steady state benzene and CO hydrogenation activities (c.c./g-Co/h) as a function of cobalt loading is shown in Fig. 6. It can be seen that for both reactions the activity decreases with increasing reduction temperature. Also for both reduction temperatures, the catalytic activity increases with increasing cobalt loading up to 3%, and levels off for higher cobalt content.

The turnover frequencies (TOF, number of cyclohexane molecules produced per site per second) for benzene hydrogenation based on cobalt dispersion calculated from both H_2 chemisorption (activated) and ESCA data are plotted in Fig. 7 as a function of cobalt loading. It can be seen that the TOF(ESCA) values ($0.1–1.5 \times 10^{-2}$ s^{-1}) are lower than the corresponding TOF(H_2)

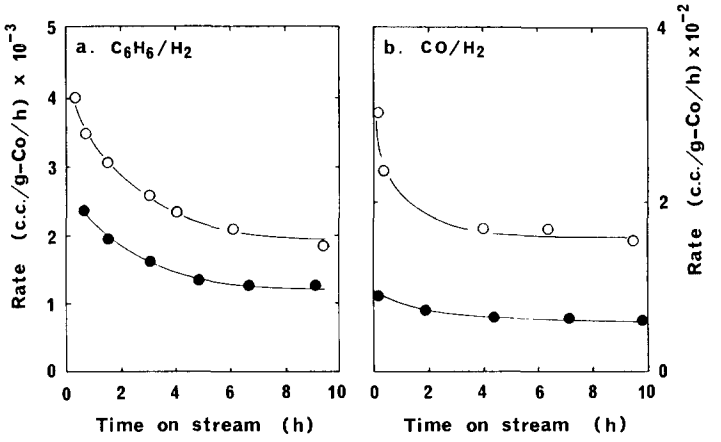

Fig. 5. Variation of catalytic activity of Co3Ti catalyst as a function of time on stream for benzene hydrogenation (a) and CO hydrogenation (b). (○), catalyst reduced at 400°C; (●), catalyst reduced at 500°C.

TABLE 6

Activity of Co/TiO_2 for Benzene Hydrogenation at 70°C

Sample	Reduction temp. 400°C			Reduction temp. 500°C		
	Rate[a]	TOF[b] × 10^2		Rate[a]	TOF[b] × 10^2	
		ESCA	H_2		ESCA	H_2
Co0.5Ti	702 ± 104[c]	0.3		520 ± 163	0.2	
	455 ± 73[d]	0.2		312 ± 72	0.1	
Co1Ti	1700 ± 141	0.6		1225 ± 35	0.5	
	1034 ± 189	0.4		600 ± 180	0.2	
Co1.5Ti	2046 ± 77	1.1	8.5	1472 ± 154	0.8	12.3
	1290 ± 297	0.6	5.4	850 ± 85	0.5	7.1
Co3Ti	3139 ± 86	1.9	10.5	1919 ± 256	1.3	12.8
	1772 ± 40	1.1	5.9	1100 ± 141	0.7	7.3
Co4Ti	3035 ± 233	2.4	8.4	1686 ± 161	1.2	10.2
	1800 ± 140	1.4	5.0	951 ± 69	0.7	5.8
Co6Ti	3013 ± 159	2.5	6.7	1630 ± 32	1.4	6.8
	1851 ± 35	1.5	4.1	1027 ± 76	0.9	4.3

[a] Rate in c.c./g-Co/h.
[b] TOF (s^{-1}) was calculated from cobalt dispersion measured by ESCA and H_2 chemisorption.
[c] Activity after 2 min on stream.
[d] Activity after 8 h on stream (steady state).

TABLE 7

Activity of Co/TiO_2 for CO Hydrogenation at 185°C

Sample	Reduction temp. 400°C			Reduction temp. 500°C		
	Rate[a]	TOF[b] × 10^3		Rate[a]	TOF[b] × 10^3	
		ESCA	H_2		ESCA	H_2
Co0.5Ti	97 ± 22[c]	0.4		38 ± 7	0.14	
	52 ± 11[d]	0.2		16 ± 3	0.06	
Co1Ti	178 ± 12	0.9		45 ± 13	0.2	
	85 ± 13	0.4		33 ± 4	0.1	
Co1.5Ti	256 ± 2	1.3	10.7	48 ± 3	0.3	4.0
	124 ± 4	0.6	5.2	40 ± 2	0.2	3.0
Co3Ti	330 ± 13	2.1	11.0	94 ± 4	0.6	6.3
	165 ± 3	1.0	5.5	64 ± 6	0.4	4.3
Co4Ti	338 ± 42	2.7	9.4	102 ± 11	0.8	6.2
	169 ± 5	1.3	4.7	76 ± 5	0.6	4.6
Co6Ti	322 ± 25	2.7	7.2	108 ± 1	0.9	4.5
	152 ± 11	1.3	3.4	75 ± 2	0.6	3.1

[a] Rate in c.c./g-Co/h.
[b] TOF (s^{-1}) was calculated from cobalt dispersion measured by ESCA and H_2 chemisorption.
[c] Activity after 1 h on stream.
[d] Activity after 8 h on stream (steady state).

values (4–7 × 10^{-2} s^{-1}) for all catalysts. In addition, the TOF(ESCA) increases with increasing cobalt loading and reduction temperature, whereas the TOF(H_2) shows little variation with cobalt content or reduction treatment.

The variation of TOF for CO hydrogenation as a function of cobalt loading is shown in Fig. 8. Note that the TOFs(H_2) (3–5 × 10^{-3} s^{-1}) are higher than the TOFs(ESCA) (0.1–1.3 × 10^{-3} s^{-1}). The observed variation of TOF(ESCA) with cobalt content is similar to that obtained for benzene hydrogenation.

The variation of TOF(ESCA) as a function of cobalt dispersion (from ESCA data) at the two reduction temperatures is shown in Fig. 9 for benzene and CO hydrogenation. A decrease in TOF(ESCA) with in-

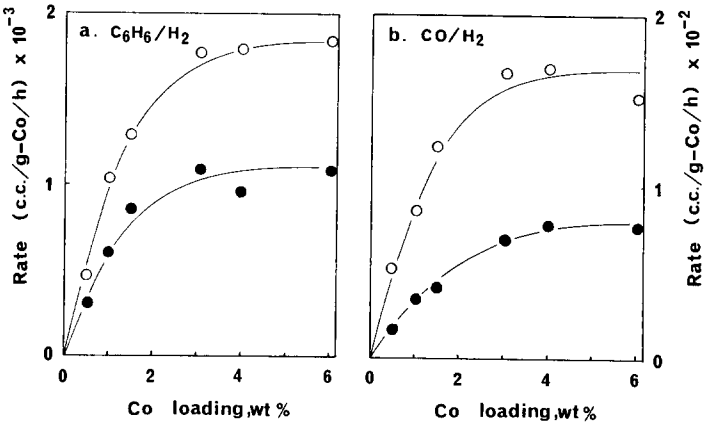

Fig. 6. Variation of catalytic activity for benzene hydrogenation (a) and CO hydrogenation (b) as a function of cobalt loading. (○), catalysts reduced at 400°C; (●), catalysts reduced at 500°C.

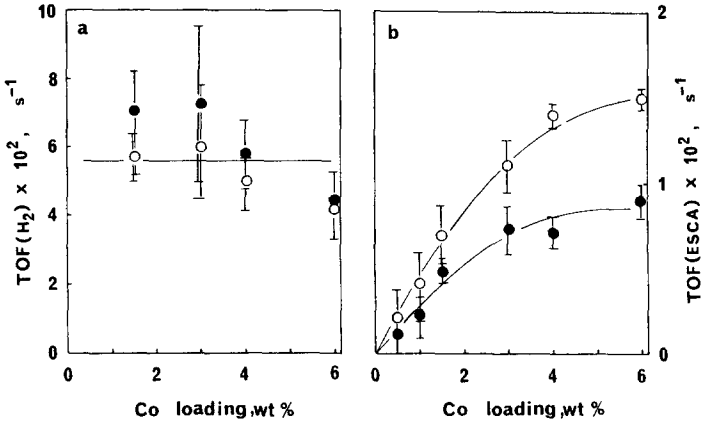

Fig. 7. Variation of turnover frequency, TOF(H_2) (a) and TOF(ESCA) (b), for benzene hydrogenation as a function of cobalt loading. (○), catalysts reduced at 400°C; (●), catalysts reduced at 500°C.

creasing reduction temperature and cobalt dispersion is observed for both reactions.

DISCUSSION

The Chemical State and Dispersion of Cobalt

For Co0.5Ti and Co1Ti catalysts, the agreement between the experimental ESCA Co2$p_{3/2}$/Ti2p intensity ratios and the predicted monolayer values indicates that the cobalt phase is primarily present as a highly dispersed surface cobalt species on these catalysts. The Co2$p_{3/2}$ binding energy (781.2 ± 0.2 eV) and the shake-up satellite intensity are consistent with the presence of surface $CoTiO_3$. The formation of $CoTiO_3$ in Co/TiO_2 catalysts has been reported for catalysts calcined at 650°C (*26*).

For cobalt loadings higher than 1%, the observed ESCA Co2$p_{3/2}$/Ti2p intensity ratios were significantly lower than the predicted monolayer values. This indicates that discrete cobalt particles were formed, in accord with the observation of XRD lines of Co_3O_4. The decrease in the relative shake-up satellite intensity of the Co2$p_{3/2}$ peak with increasing cobalt loading and in

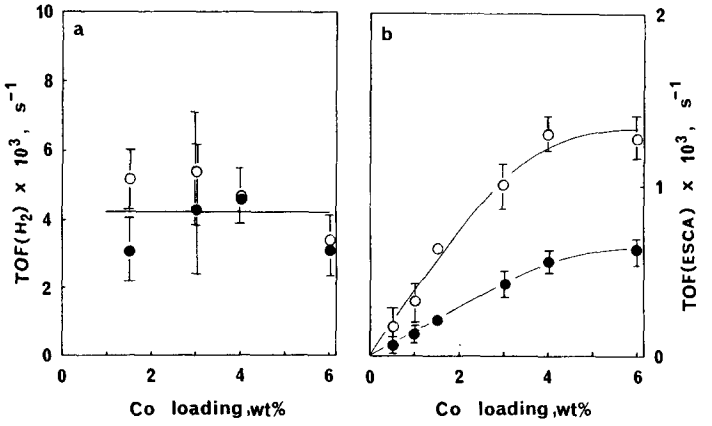

Fig. 8. Variation of turnover frequency, TOF(H_2) (a) and TOF(ESCA) (b), for CO hydrogenation as a function of cobalt loading. (○), catalysts reduced at 400°C; (●), catalysts reduced at 500°C.

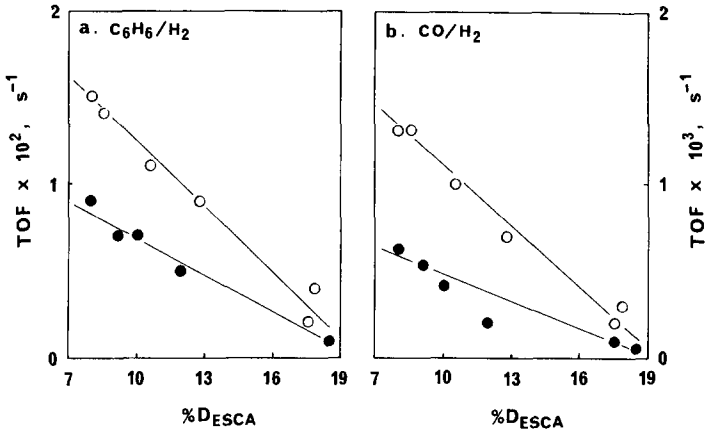

Fig. 9. Variation of turnover frequency, TOF(ESCA), as a function of cobalt dispersion (ESCA) for benzene hydrogenation (a) and CO hydrogenation (b). (○), catalysts reduced at 400°C; (●), catalysts reduced at 500°C.

the Co2$p_{3/2}$ binding energy from 781.2 to 780.0 eV are also consistent with the formation of Co_3O_4. It is worth noting that for Co loadings higher than 1 wt%, the ESCA Co/Ti intensity ratios decrease to values lower than that measured for Co1Ti. In fact, the measured intensity ratios for Co loadings ≥3 wt% were comparable to that obtained for Co0.5Ti. This behavior cannot be simply attributed to the formation of discrete Co particles on top of the atomically dispersed phase present in the Co1Ti catalyst, since such distribution of the Co phase should lead to a leveling off of the ESCA Co/Ti intensity ratios around a value at least equal to that measured for the Co1Ti catalyst. One interpretation for the observed decline in the ESCA Co/Ti intensity ratios for Co loadings higher than 1 wt% (assuming that all samples are uniform) is a decrease in the absolute amount of Co present as a surface compound. This could be attributed to a greater ease of nucleation of the Co_3O_4 phase from concentrated Co solutions at the detriment of the surface phase.

The fraction of cobalt present as the Co(II) surface species (x) can be estimated by curve fitting the ESCA Co2$p_{3/2}$ envelope according to the modified ESCA method (*23*). Assuming that Co(II) and Co_3O_4 are the only Co phases present, the fraction of the cobalt phase present as Co_3O_4 (i.e., 1-x) can readily be obtained. The results are shown in Fig. 10. It can be seen that as cobalt loading increases from 0.5 to 3%, the percent of Co(II) decreases from 100 to 10%. Further addition of cobalt has no significant effect on the relative amount of cobalt species. Also reported in Fig. 10 is the percent of Co_3O_4 estimated from quantitative XRD. There is a fairly good agreement between the two techniques.

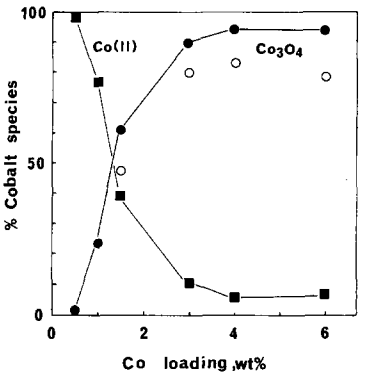

Fig. 10. The distribution of cobalt phases as a function of cobalt loading in the oxidic catalysts. (■), Co(II); (●), Co_3O_4 (ESCA); (○), Co_3O_4 (XRD).

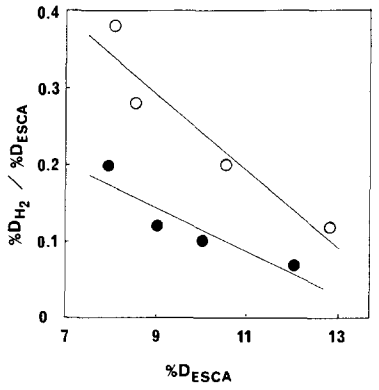

Fig. 11. Variation of the fraction of surface cobalt atoms which chemisorb hydrogen, $[\%D_{H2}/\%D_{ESCA}]$, versus cobalt dispersion (ESCA). (○), catalysts reduced at 400°C; (●), catalysts reduced at 500°C.

Evidence for the Reduction of TiO_2 and Suppression of H_2 Chemisorption

Partial reduction of TiO_2 at temperatures above 400°C inferred from oxygen titration is in agreement with other studies (*20–22, 25*). Additional reduction of TiO_2 occurred when cobalt metal was present, indicating that cobalt metal facilitates the reduction of TiO_2. This has been attributed to hydrogen spill-over (*21*).

It is of interest to compare the apparent dispersion of the cobalt phase obtained from H_2 chemisorption with that estimated from the cobalt particle size values determined by ESCA. The ratio $[\%D_{H2}/\%D_{ESCA}]$ represents the fraction of "surface" cobalt which chemisorbs hydrogen. Figure 11 shows a plot of $[\%D_{H2}/\%D_{ESCA}]$ as a function of cobalt dispersion (obtained from ESCA) for the two reduction temperatures. The decrease in $[\%D_{H2}/\%D_{ESCA}]$ with increasing cobalt dispersion agrees with the reported effect of crystallite size on the onset of SMSI for titania supported nickel catalysts (*27*). Also, the decrease in $[\%D_{H2}/\%D_{ESCA}]$ with increasing reduction temperature parallels the increase of TiO_2 reduction determined from oxygen titration (see Table 4). This is consistent with the explanation that the suppression of hydrogen chemisorption is caused by covering of the active metal surface with reduced TiO_x species (*28*). The amount of TiO_x needed to cover completely the cobalt surface (assuming that one TiO_x moiety is required to cover one cobalt atom) was calculated to be less than 30% of the Ti^{+3} ions generated in the Co6Ti catalyst after reduction at 500°C (see Table 4). Assuming that Ti^{+3} ions formed are atomically dispersed on the support surface, the surface reduction of TiO_2 can be estimated. A maximum amount of 30% surface reduction was calculated for the Co6Ti catalyst reduced at 500°C. This corresponds to ca. 5% contribution from Ti^{+3} to the total ESCA Ti2*p* area based on the Kerkhof and Moulijn model (*13*). A computer composite made from $Ti2p_{3/2}$ spectra characteristic of Ti^{+4} and Ti^{+3} indicates no observable change in the Ti2*p* envelope for such a minor contribution of Ti^{+3}, which is consistent with the experimental results.

Effect of Reduction Temperature and Cobalt Dispersion on Benzene and CO Hydrogenation Activities

The observed decrease in the TOF (ESCA) of Co/TiO_2 catalysts for benzene hydrogenation with increasing reduction temperature is similar to the results reported by Marcelin *et al.* for modified aluminum phosphate-supported nickel catalysts (*29*). These authors noted that the decrease in TOF (based on Ni particle size obtained from XRD line broadening) correlates with the suppression in the capacity of Ni to adsorb hydrogen at high reduction temperature. The results were interpreted as an indication that only Ni sites which chemisorb hydrogen are catalytically active. This was illustrated by a constant TOF calculated from H_2 chemisorption. Our results, indeed, show that a correlation exists between TOF(ESCA) and the fraction of surface cobalt which chemisorbs hydrogen $[\%D_{H2}/\%D_{ESCA}]$ (Fig. 9a and 11). Also, the observed $TOF(H_2)$ (5.6 ± 1.2 s^{-1}) for benzene hydrogenation appears to be little

affected by the reduction temperature and cobalt dispersion. Therefore, in line with the explanation proposed for the $Ni/AlPO_4$ system, the decrease in benzene hydrogenation activity can be attributed mainly to the decrease in the number of surface cobalt atoms which can chemisorb hydrogen.

The variation of TOF(ESCA) for Co/TiO_2 catalysts for CO hydrogenation with increasing reduction temperature and cobalt dispersion is similar to that observed for benzene hydrogenation. Burch and coworkers (*30, 31*) proposed that high temperature reduction of Ni/TiO_2 catalysts leads to migration of TiO_x species onto the surface of metal particle, which may create new active sites and/or physically block some of the metal surface. From this model, the observed activity is the balance of these two opposing factors. Clearly, our results which show TOF(ESCA) values decreasing with increasing reduction temperature and cobalt dispersion (Fig. 9b), and $TOF(H_2)$ values ($4.2 \pm 1\ s^{-1}$) practically constant (Fig. 8a) mainly reflect a decrease in the number of exposed cobalt atoms due to site blocking by reduced TiO_x. The similar catalytic behavior of Co/TiO_2 for benzene and CO hydrogenation as a function of reduction temperature and cobalt dispersion (Figs. 7, 8, and 9) is consistent with this explanation.

CONCLUSIONS

ESCA and XRD indicate that the cobalt phase in oxidic Co0.5Ti and Co1Ti catalysts is present as highly dispersed surface $CoTiO_3$. For catalysts having higher cobalt loadings, discrete Co_3O_4 particles are formed in addition to surface $CoTiO_3$. The relative amount of Co_3O_4 increases as the cobalt loading increases to 3% and levels off for higher loadings.

ESCA indicates that the cobalt metal particle size increases as the cobalt loading increases, and remains essentially unchanged as a function of reduction temperature from 400 to 500°C.

Hydrogen chemisorption is found to be activated; the extent of activation is a function of cobalt loading and reduction temperature. Furthermore, cobalt capacity for hydrogen chemisorption is suppressed; the fraction of "surface" cobalt atoms which chemisorb hydrogen decreases as the reduction temperature is increased and as the cobalt metal particle size is decreased.

The TOF's(ESCA) for benzene and CO hydrogenation were found to decrease with increasing reduction temperature (400–500°C) and decreasing cobalt particle size. The decline in activity correlates with the extent of suppression of hydrogen chemisorption. The results were interpreted in terms of a decrease in the fraction of exposed surface cobalt due to site blocking by reduced TiO_x moieties.

ACKNOWLEDGMENTS

This work was supported by the National Science Foundation under Grant CHE-8401202. Sui-Wen Ho acknowledges the National Science Council, Republic of China, for a Predoctoral Fellowship.

REFERENCES

1. Tauster, S. J., Fung, S. C., and Garten, R. L., *J. Am. Chem. Soc.* **100,** 170 (1978).
2. Meriaudeau, P., Ellestad, O. H., Dufaux, M., and Naccache, C., *J. Catal.* **75,** 243 (1982).
3. Vannice, M. A., *J. Catal.* **74,** 199 (1982).
4. Stevenson, S. A., *et al.*, Eds., "Metal–Support Interaction in Catalysis, Sintering, and Redispersion," Van Nostrand–Reinhold, New York, 1987.
5. Viswanathan, B., and Gopalakrishman, R., *Curr. Sci.* **55,** 32 (1986).
6. Del Arco, M., and Rives, V., *J. Mater. Sci.* **21,** 2938 (1986)
7. Lisitsyn, A. S., Golovin, A. V., Kuznetsov, V. L., and Yermakov, Y. I., *Cl Mol. Chem.* **1,** 115 (1984).
8. Reuel, R. C., and Bartholomew, C. H., *J. Catal.* **85,** 78 (1984).
9. Lee, J-H., Lee, D-K., and Ihm, S-K., *J. Catal.* **113,** 544 (1988).
10. Klug, H. P., and Alexander, I. E., "X-ray Diffraction Procedures," pp. 385. Wiley, New York, 1954.
11. Fung, S. C., *J. Catal.* **58,** 454 (1979).
12. Defosse, C., *J. Electron Spectrosc. Relat. Phenom.* **23,** 157 (1981).
13. Kerkhof, F. P. J. M., and Moulijn, J. A., *J. Phys. Chem.* **83,** 1612 (1979).

14. Scofield, J. H., J. *Electron Spectrosc. Relat. Phenom.* **8,** 129 (1976).
15. Penn, D. R., *J. Electron Spectrosc. Relat. Phenom.* **9,** 29 (1976).
16. Zowtiac, J. M., and Bartholomew, C. H., *J. Catal.* **83,** 107 (1983).
17. Bartholomew, C. H., and Farrauto, R. J., *J. Catal.* **45,** 41 (1976).
18. Criado, J., and Real, C., *J. Chem. Soc. Faraday Trans. 1* **79,** 2765 (1983).
19. Frost, D. C., Mcdowell, C. A., and Woolsey, I. S., *Mol.* Phys. **27,** 1473 (1974).
20. Fernandez, A., Leyrer, J., Gonzalez-Elipe, A. R., Munuera, G., and Knozinger, H., *J. Catal.* **112,** 489 (1988).
21. Sexton, B. A., Hughes, A. E., and Foger, K., *J. Catal.* **77,** 85 (1982).
22. Chien, S-H., Shelimov, B. N., Resasco, D. E., Lee, E. H., and Haller, G. L., *J. Catal.* **77,** 301 (1982).
23. Stranick, M. A., Houalla, M., and Hercules, D. M., *J. Catal.* **103,** 151 (1987).
24. Castner, D. G., and Stantilli, D. S., *ACS Sym. Ser.* **248,** 39 (1984).
25. Huizinga, T., Von Grondelle, J., and Prins, R., *Appl. Catal.* **10,** 199 (1984).
26. Tohji, K., Udagawa, Y., Tanabe, S., Ida, T., and Ueno, A., *J. Am. Chem. Soc.* **106,** 5172 (1984).
27. Ko, E. I., Winston, S., and Woo, C., *J. Chem. Soc. Chem. Commun.* 740 (1982).
28. Santos, J., Phillips, J., and Dumesic, J. A., *J. Catal.* **81,** 147 (1983).
29. Marcelin, G., Vogel, R. F., and Swift, H. E., *J. Catal.* **98,** 64 (1986).
30. Anderson, J. B. F., Bracey, J. D., Burch, R., and Flambard, A. R., *in* "Proceedings 8th International Congress on Catalysis, Berlin, 1984," Vol. V. p. 111. Dechema, Frankfurt-am-Main, 1984.
31. Burch, R., and Flambard, A. R., *J. Catal.* **85,** 16 (1984).